Received: 25 March 2020 | Revised: 2 July 2020 | Accepted: 3 July 2020

DOI: 10.1002/glia.23890

GLIA

WILEY

RESEARCH ARTICLE

Phagocytosis-related NADPH oxidase 2 subunit gp91phox contributes to neurodegeneration after repeated systemic challenge with lipopolysaccharides

Anahita Shahraz[1] | Jannis Wißfeld[1] | Aurélien Ginolhac[2] | Mona Mathews[1] | Lasse Sinkkonen[2] | Harald Neumann[1]

[1]Institute of Reconstructive Neurobiology, Medical Faculty and University Hospital of Bonn, University of Bonn, Venusberg-Campus 1, Bonn, 53127, Germany

[2]Department of Life Sciences and Medicine, University of Luxembourg, 6, avenue du Swing, Belvaux, L4367, Luxembourg

Correspondence
Harald Neumann, Neural Regeneration Unit, Institute of Reconstructive Neurobiology, Medical Faculty and University Hospital of Bonn, University of Bonn, Venusberg-Campus 1, Bonn 53127, Germany.
Email: harald.neumann@uni-bonn.de

Abstract

Repeated systemic challenge with lipopolysaccharides (LPS) can induce microglia activation and inflammatory neurodegeneration in the substantia nigra pars compacta region of mice. We now explored the role of mononuclear phagocytes associated nicotinamide adenine dinucleotide phosphate oxidase 2 (NOX-2) in inflammatory neurodegeneration. *Cybb*-deficient NOX-2 knock-out (KO) and control wild type (WT) mice were treated intraperitoneally daily over four consecutive days with 1 μg/gbw/day LPS. Transcriptome analysis by RNA-seq of total brain tissue indicated increased LPS-induced upregulation of genes belonging to the reactive oxygen species and reactive nitrogen species production, complement and lysosome activation as well as apoptosis and necroptosis in WT compared to NOX-2 KO mice. Validation of up-regulated gene transcripts via qRT-PCR confirmed that LPS-challenged NOX-2 KO mice expressed lower levels of the microglial phagocytosis-related genes *Nos2*, *Cd68*, *Aif1/Iba1*, *Cyba*, *Itgam*, and *Fcer1g* compared to WT mice at Day 5 after systemic inflammatory challenge, but no significant differences in the pro-inflammatory genes *Tnfα* and *Il1b* as well as microglial IBA1 and CD68 intensities were observed between both genotypes. Furthermore, loss of tyrosine hydroxylase positive (TH+) and NeuN positive neurons in the substantia nigra pars compacta upon repeated systemic LPS application were attenuated in NOX-2 KO mice. Thus, our data demonstrate that loss of dopaminergic neurons in the substantia nigra pars compacta after repeated systemic challenge with LPS is associated with a microglial phagocytosis-related gene activation profile involving the NADPH oxidase subunit Cybb/gp91phox.

KEYWORDS

lipopolysaccharides, microglia, NADPH oxidase, neurodegeneration, neuroinflammation, phagocytes, radicals

1 | INTRODUCTION

Systemic inflammation associated with bacterial infections can exacerbate chronic neurodegenerative processes (Perry, Cunningham, & Holmes, 2007; Wyss-Coray & Rogers, 2012). Particularly, dopaminergic neurons in the substantia nigra (SN) are susceptible to pro-inflammatory and oxidative damage. Therefore, systemic lipopolysaccharides (LPS) injections in mice have been used to provide valuable insights into the potential contribution of inflammatory stimuli to Parkinson's disease (PD). Systemic single application of a sublethal dose of LPS in mice caused chronic inflammation in the brain and progressive delayed loss of nigral tyrosine hydroxylase positive (TH+) neurons (Qin et al., 2007). Furthermore, repeated intraperitoneal LPS injections over 4 days with 1 μg/gbw/day induced a rapid increase in proinflammatory cytokine and immune activation gene transcription in the brain followed by dopaminergic neurodegeneration in the substantia nigra pars compacta (SN*pc*) at 19 days that was mediated via a complement pathway involving complement factor C3 (Bodea et al., 2014).

Other studies confirmed the contribution of innate immune activation as well as a role of nitric oxide to dopaminergic neuron loss in the midbrain (Czapski, Cakala, Chalimoniuk, Gajkowska, & Strosznajder, 2007; Zheng et al., 2013). Furthermore, it was shown that NOX-2 KO compared to wildtype control mice showed no loss of neurons in the substantia nigra compared to control mice after an extended time period of 10 months following a single intraperitoneal administration of LPS (5 μg/gbw, i.p.) (Qin, Liu, Hong, & Crews, 2013), indicating a possible involvement of phagocytic NADPH oxidases in loss of dopaminergic neurons. NADPH oxidase complex activation can lead to release of superoxide (O_2^-), which could react with nitric oxide (NO) to form peroxynitrite, which has a very high potential to oxidize lipids and proteins. However, the exact contribution of the phagocytic NADPH oxidases to neurodegeneration in the substantia nigra triggered by repeated systemic application of LPS is still unclear.

Here we show that nigrostriatal neurodegeneration already visible 19 days after repeated systemic application of LPS is prevented in mice deficient for the subunit *Cybb/gp91phox* of the NADPH oxidase 2 (NOX-2). Furthermore, NOX-2 KO mice show less *Cd68*, *Aif1/Iba1*, *Nos2*, *Cyba*, *Itgam*, and *Fcer1g* gene transcription after repeated systemic LPS challenge, indicating involvement of a broad phagocytosis-related mechanism in neuronal loss.

2 | MATERIAL AND METHODS

2.1 | Experimental animals and treatments

Three months old male wild type (WT) mice (C57BL/6J, originally obtained from Charles River and bred in our animal facility) or $gp91^{phox-}$ (NOX-2 KO, B6.129S-Cybbtm1Din/J, originally from The Jackson Laboratory and back-crossed for at least 10 generations in C57BL/6J) mice were used throughout this study. The animals were housed in a specific-pathogen-free environment and had free access to water and food ad libitum. For experiments, mice (selected randomly to each group after they reached the age of 12-weeks) were intraperitoneally injected daily, and repeatedly over four consecutive days, with either 100 μl lipopolysaccharides (LPS; *Salmonella abortus equi* S-form; Cat # ALX-581-009-002; Enzo Life Science; 1 μg/gbw/day,) or 100 μl PBS/day as vehicle control. Repeated injections were performed as previously described (Bodea et al., 2014). The injections were done in four consecutive days and the analysis was performed on the fifth day or 19th day after the first day of injection. All experiments were approved by authors institutional review boards and by the local governmental authorities and have been done according to the principles expressed in the Helsinki Declaration.

2.2 | RNA isolation

Animals were deeply anesthetized, killed and perfused intracardially with 1× PBS. Brains were collected and divided to two halves. Left hemispheres were immediately homogenized in 1 ml QIAzol (QIAGEN) and RNA was isolated according to the manufacturer's protocol. Following a chloroform step, RNA was precipitated with isopropanol and the RNA pellet washed twice with 75% ethanol. After air-drying, the RNA was re-suspended in DEPC water and the RNA concentration was measured by NanoDrop 2000 spectrophotometer (ThermoScientific).

2.3 | Semi-quantitative real-time PCR analysis

Reverse transcription of 5 μg total RNA was performed with superscript III reverse transcriptase (Invitrogen) and hexamer random primers (Sigma). Semi-quantitative RT-PCR was performed using 200 ng cDNA, SYBR® GreenER™ qPCR SuperMix Universal (ThermoScientific) and specific oligonucleotides were added into a final reaction volume of 25 μl. For PCR-amplifications, a Mastercycler ep Gradient S (Eppendorf) was used, and the results were evaluated by manufacturer's software. Amplification specificity was confirmed by melting curve analysis, and the quantification of the obtained PCR products was performed by the ΔΔCt method with *Gapdh* as internal reference gene. In total, 10 pmol of the following primer pairs were used in real-time reactions:

Gapdh F- AACTTTGGCATTGTGGAAGG, R-GGATGCAGGGATGATGTTCT;

Cd68 F-CAGGGAGGTTGTGACGGTAC, R-GAAACATGGCCCGAAGTATC;

Iba1 F-GAAGCG AATGCTGGAGAAAC, R-AAGATGGCAGATCTCTTGCC;

Tmem119 F-GTGTCTAACAGGCCCCAGAA, R-AGCCACGTGGTATCAAGGAG;

Nos-2 F-AAGCCCCGCTACTACTCCAT, R-GCTTCAGGTTCCTGATCCAA;

Cyba F-CCTCCACTTCCTGTTGTCGG, R-TCACTCGGCTTCCTTTCGGAC;

Cybb F-GGGAACTGGGCTGTGAATGA, R-CAGTGCTGACCCAA GGAGTT;

Tnfα F-TCTTCTCATTCCTGCTTGTGG, R-AGGGTCTGGGCCAT AGAACT;

Il1β F-CTTCCTTGTGCAAGTGTCTG, R-CAGGTCATTCTCATC ACTGTC;

Dap12 F-ACAGCGGAAGGGACCCGGAAA, R-TCAGGCCGCTG ATGGGCATA; *Fcer1g* F-CTGTCTACACGGGCCTGAAC, R-AAAGAA TGCAGCCAAGCACG;

C3 F-TAGTGCTACTGCTGCTGTTGGC, R-GCTGGAATCTTGAT GGAGACGCTT; *Itgam* F-AATTGGGGTGGGAAATGCCT, R-TGGT ACTTCCTGTCTGCGTG;

C4 F-TGGAGGACAAGGACGGCTA, R- GGCCCTAACCCTGAG CTGA.

Bad F- ACATTCATCAGCAGGGACGG, R- ACTCATCGCTCA TCCTTCGG;

Casp8 F- TGGAGAAGAGGACCATGCTG, R- AGTCACACAGTTC CGCCATT;

Cd14 F- TGTGGACACGGAAGCAGATC, R- CGTTGCGGAG GTTCAAGATG;

Erk1 F- GTCTCTGCCCTCGAAAACCA, R- ATCAACTCCTTCAG CCGCTC;

Fadd F- GTGGCCTGGACCTGTTCAC, R- GGGCCAGTCTTT TCCAGTCT;

Mlkl F- CAAACAGTGAAGCCCCCTGA, R- AGCTGCTGATGTT TCTGTGGA;

Myd88 F- ACAAACGCCGGAACTTTTCG, R- GAAACAACCACC ACCATGCG;

Pik3cd F- GTCCACTCCTCCTCCATCCT, R- CAGCATTCACTTT TCGGCCC;

Ripk1 F- TGTACCCTTACCTCCGAGCA, R- GGCTGCGGTTTTGT CTGTTT;

Ripk3 F- TTCCAGGACTGCGAACCAAA, R- TCTTTGGCTTGGCTC TCTGG;

Th F- TGAAGGAACGGACTGGCTTC, R- CCTGGGAGAACTGG GCAAAT;

Tlr4 F- AGATCTGAGCTTCAACCCCTTG, R- TCCACAGCCACCA GATTCTC.

2.4 | Immunohistochemistry

Brains were collected as described above and the right hemispheres were kept in ice cold 4% paraformaldehyde (PFA; Sigma) for at least 24 hr at 4°C. Afterward brains were moved into 30% sucrose (Sigma) supplemented with 0.1% sodium azide (Sigma) and kept at 4°C until processed into frozen cryosections. Fixed brains were sectioned in coronal plane (20 μm extent in the rostral-caudal plane) and directly mounted onto superfrost slides. Slides containing ventral midbrain region were blocked with PBS containing 10% bovine serum albumin (Roth), 5% normal goat serum (Sigma) and 0.2% triton X-100 (Sigma) followed by 2 hr incubation with primary antibodies. After washing with 1× PBS, the slices were incubated with corresponding secondary antibodies for 2 hr at room temperature (Cy3-conjugated antibody, 1:500, Dianova or Alexa-488-conjugated antibody, Invitrogen). Respective isotype control and secondary antibodies were used in all immunostainings in parallel to the antigen-specific staining. Slides were mounted with Mowiol (Sigma) and were kept in 4°C until images were taken. Staining of the different experimental groups were done as one experiment, and images were recorded using the same settings of an AxioObserver Z1 inverted microscope equipped with an AxioCam MRm camera, Apotome feature and AxioVision software (Carl Zeiss). The images were collected via 10x objective with mosaic function of the microscope, in a fixed set up of 15 images (×3 horizontal and ×5 vertical). Afterward, the images were stitched together by the software and converted to adjust the overlaps. Hereby one final "composite image" from one section was obtained. Analysis of the "composite image" was performed via the ImageJ software, in which the area of Substantia nigra *pars compacta* (SN*pc*) was selected for counting of stained cells. For neuronal quantifications, slides were double stained with primary antibodies directed against dopaminergic neurons marker tyrosine hydroxylase (TH) (1:500; Sigma) and against neuronal nuclei marker NeuN (1:500; Millipore). SN*pc* areas were recognized according to the TH-positive immunostaining as described before (Bodea et al., 2014). Optical sections for SN*pc* matched levels (bregma −2.92, −3.28, and −3.52 mm) per animal were used for cell counting. For microglial activation, double stainings of the lysosomal marker CD68 (1:500, Serotec) and IBA1-positive microglia (1:1,000, Wako) were quantified from the substantia nigra pars reticulata (SN*pr*). Images from the controls were used to set the background staining to a minimum and then recorded with the same microscope settings as the antigen-specific immunostainings. Confocal z-stack images were acquired, and the areas occupied by CD68-positive staining were analyzed. At least three images per animal were analyzed.

2.5 | RNA sequencing, differential expression, and pathway analysis

Total RNA for RNA sequencing was extracted as described above. Library preparation (QuantSeq 3' mRNA-Seq Library Prep Kit, Lexogen) with an input of 100 ng total RNA, quality control (Tapestation 2200, Fa. Agilent) and RNA sequencing were performed at the NGS Core Facility, University Hospital of Bonn, with 1×10^7 single-end reads per sample on a HiSeq 2500 V4. Reads were aligned to the mouse reference genome mm10 (GRCm38.p6) with the ensemble gene annotation version 98 using STAR [v2.7.3a (Dobin et al., 2013)] with standard parameters and—outFilterScoreMinOverLread 0.3—outFilterMatchNminOverLread 0.3. Read count generation was performed using featureCounts/Subread [v2.0.0 (Liao, Smyth, & Shi, 2014)] ignoring multimapping reads. Differential expression analysis was performed with R [v3.6.1 (R Core Team, 2008)] in RStudio [v1.2.1335 (RStudio Team, 2015)] using the DESeq2 package [v1.26.0 (Love, Huber, & Anders, 2014)] with the contrasts of either WT versus NOX-2 KO (factor genotypes) or PBS versus LPS (factor treatment).

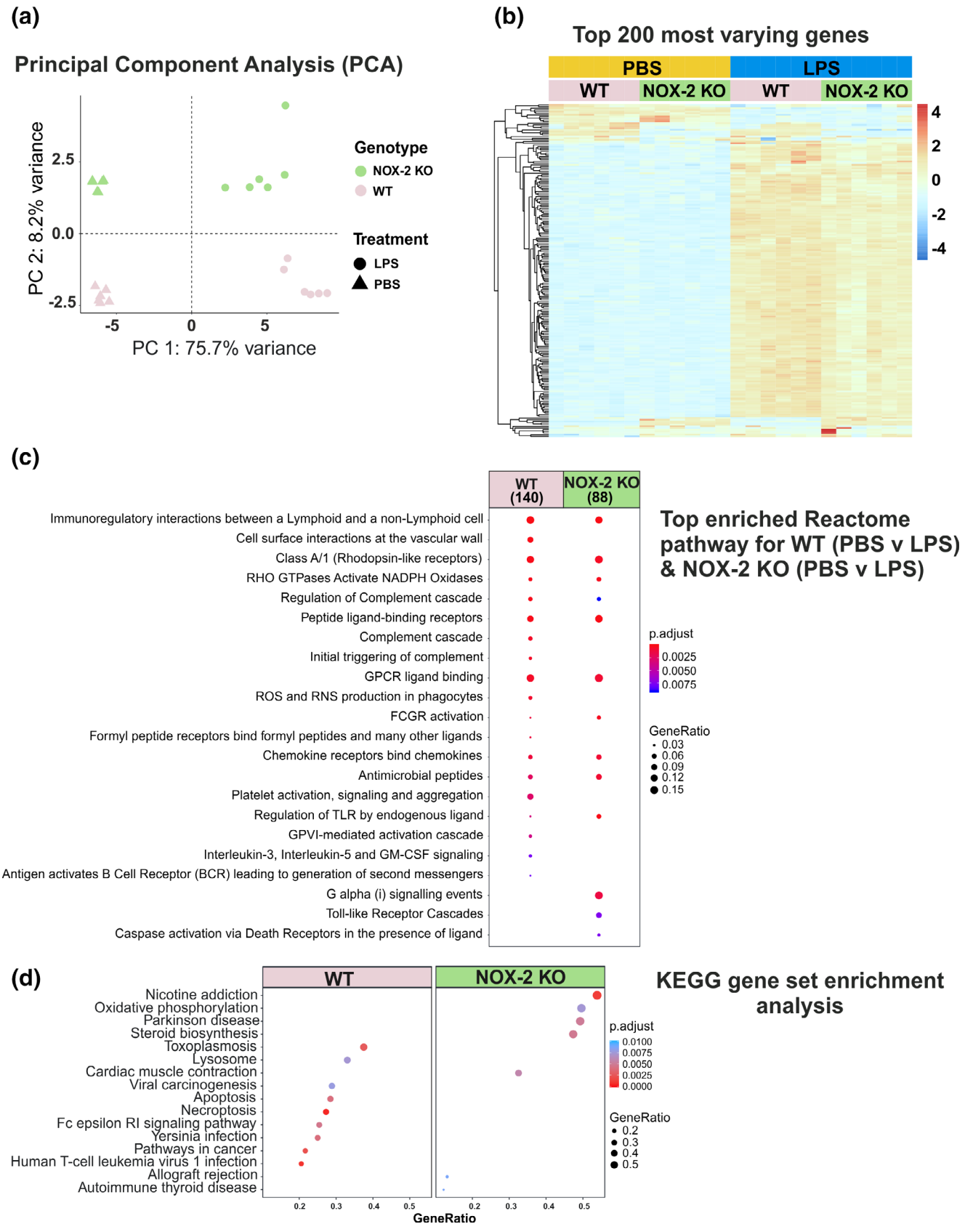

FIGURE 1 Legend on next page.

The log_2-fold change (log_2FC) shrinkage was performed using apeglm to preserve large effects of true positives [v1.8.0 (Zhu, Ibrahim, & Love, 2019)]. Transcript annotations were retrieved using the Bioconductor org.Mm.eg.db package [v3.10.0 (Carlson, 2019)] and plots were created using ggplot2 [v3.2.1 (Wickham, 2016)]. Pathway enrichment and gene set enrichment analysis were performed using clusterProfiler [v3.14.0 (Yu, Wang, Han, & He, 2012)] reactomePA [v1.30.0 (Yu & He, 2016)] and fgsea [1.12.0 (Korotkevich et al., 2019)] with log_2FC ≥ 2 and *p*adj <.01 for enrichment analysis. RNA-seq raw data are available in NCBI's Gene Expression Omnibus (GEO), under the accession number GSE153369 (https://www.ncbi.nlm.nih.gov/geo/query/acc.cgi?acc=GSE153369).

2.6 | Statistical analysis

RT-PCR and immunohistochemistry data are shown as boxplot (min./Q1/median/Q3/max.) of at least 3 independent experiments. Data were analyzed by one-way ANOVA followed by Dunnett-T3 post hoc test for significant Levene's test, or Bonferroni post hoc test for equal variances using the IBM SPSS Statistics 23.0 software. Results are considered significant as $^{*}p < .05$, $^{**}p < .01$, or $^{***}p < .001$.

3 | RESULTS

3.1 | NOX-2 specific LPS-driven brain transcriptome changes

To study the involvement of the NADPH oxidase in LPS-triggered loss of dopaminergic neurons, we compared NOX-2 KO to WT mice that were challenged repeatedly with LPS or vehicle control PBS as previously described (Bodea et al., 2014). Accordingly, LPS (1 μg/gbw/day) or PBS was applied intraperitoneally over four consecutive days and the mice were analyzed at Day 5 for neuroinflammation (Bodea et al., 2014). RNA sequencing, and subsequent analysis of differentially expressed (DE) genes and pathways, were performed from complete brain tissues to get the first insight into transcriptome changes caused by NOX-2 deficiency. Interestingly, knockout of NOX-2 in C57BL/6 mice led to only a few deregulated genes. However, despite only a few DE genes, NOX-2 KO mice were separated from WT mice by principal component analysis (Figure 1a) and hierarchical clustering (Figure 1b). A more prominent effect was observed after challenging the mice with LPS, which led to 595 DE genes in WT and 461 DE genes (log_2FC > 1, *p*adj <.05) in NOX-2 KO mice compared to the PBS injected control mice, of which most affected genes were upregulated. Since we were mainly interested in the LPS-triggered neurodegenerative effects that are NOX-2-dependent and not in any non-inflammatory effects of NOX-2, we compared the response to LPS in WT vs. NOX-2 KO mice. As expected, in both genotypes (WT and NOX-2 KO) LPS treatment mainly activated immune pathways with slight differences indicated by Reactome pathway enrichment analysis with log_2FC ≥ 2 and *p*adj <.01 (Figure 1c). Interestingly, treatment of animals with LPS led in general to a more pronounced upregulation of genes in WT mice compared NOX-2 KO mice, and in particular for the genes present in the complement cascade and radical production pathways (Figure 1c). In addition, KEGG pathway overrepresentation and gene set enrichment analysis were used to explore differences in the response of NOX-2 KO and WT animals to systemic LPS injection (Figures S1 and S2). Filtering for KEGG GSEA pathways present in only one of the two comparisons (WT or NOX-2 KO PBS vs. LPS) revealed an upregulation of phagosomal, lysosomal, apoptotic and necroptotic pathways in WT animals treated with LPS, which was partially rescued in knockout of NOX-2 (Figure 1d).

Taken together, the LPS treatment in WT led to upregulation of genes belonging to the reactive oxygen species (ROS) and reactive nitrogen species (RNS) production, complement, phagosome and lysosome activation as well as apoptosis and necroptosis pathways, which were attenuated following NOX-2 KO.

3.2 | Complement and phagocytosis-related pathways were less elevated in NOX-2 KO compared to WT mice

In the RNA-seq data, we observed a noticeable increase in complement and radical production pathways in LPS-treated WT mice in comparison to NOX-2 KO mice (Figure 1c). To have a closer look and validate this observation, we selected complement factor 3 (*C3*), integrin alpha M (*Itgam*), which is one subunit of the complement factor c3 receptor, and complement factor 4 (*C4*) to investigate the complement pathway via RT-PCR. On Day 5, the mRNA transcript levels of *C3*, *Itgam*, and *C4* were increased in LPS challenged mice compared to PBS control, in both genotypes. For *C3* in WT genotype, transcription levels increased from 1.04 ± 0.1 to 28.9 ± 3.37 (mean ± SEM; $p < .001$; Figure 2a); and in NOX-2 KO genotype this level increased from 0.84 ± 0.09 to 18 ± 1.9 (mean ± SEM; $p < .001$; Figure 2a). For *Itgam* in WT genotype, transcription levels increased from 1.02 ± 0.07

FIGURE 1 RNA sequencing analysis of WT and NOX-2 KO mice treated with LPS or vehicle control PBS. (a). Principal component analysis of WT and NOX-2 KO mice injected with LPS or PBS as control. All four groups are separated well, but the treatment (PBS or LPS) dependent separation on PC1 had a greater influence on the variance than the genotype (WT or NOX-2 KO). (b). Heatmap of the top 200 most varying genes. Hierarchical clustering of genes resulted in separation of the individual groups. Again, a greater variance was observed within the different treatments (PBS or LPS) than between the two genotypes. (c). Comparison of the top enriched Reactome pathways in WT PBS versus LPS and NOX-2 KO PBS versus LPS. Complement and radical production pathways were overrepresented in WT but not NOX-2 KO comparisons. (d). KEGG Gene set enrichment analysis filtered for pathways only present in one of the two comparisons revealed an increase in lysosomal, phagosomal, apoptotic and necroptotic pathways in WT but not NOX-2 KO LPS-injected animals

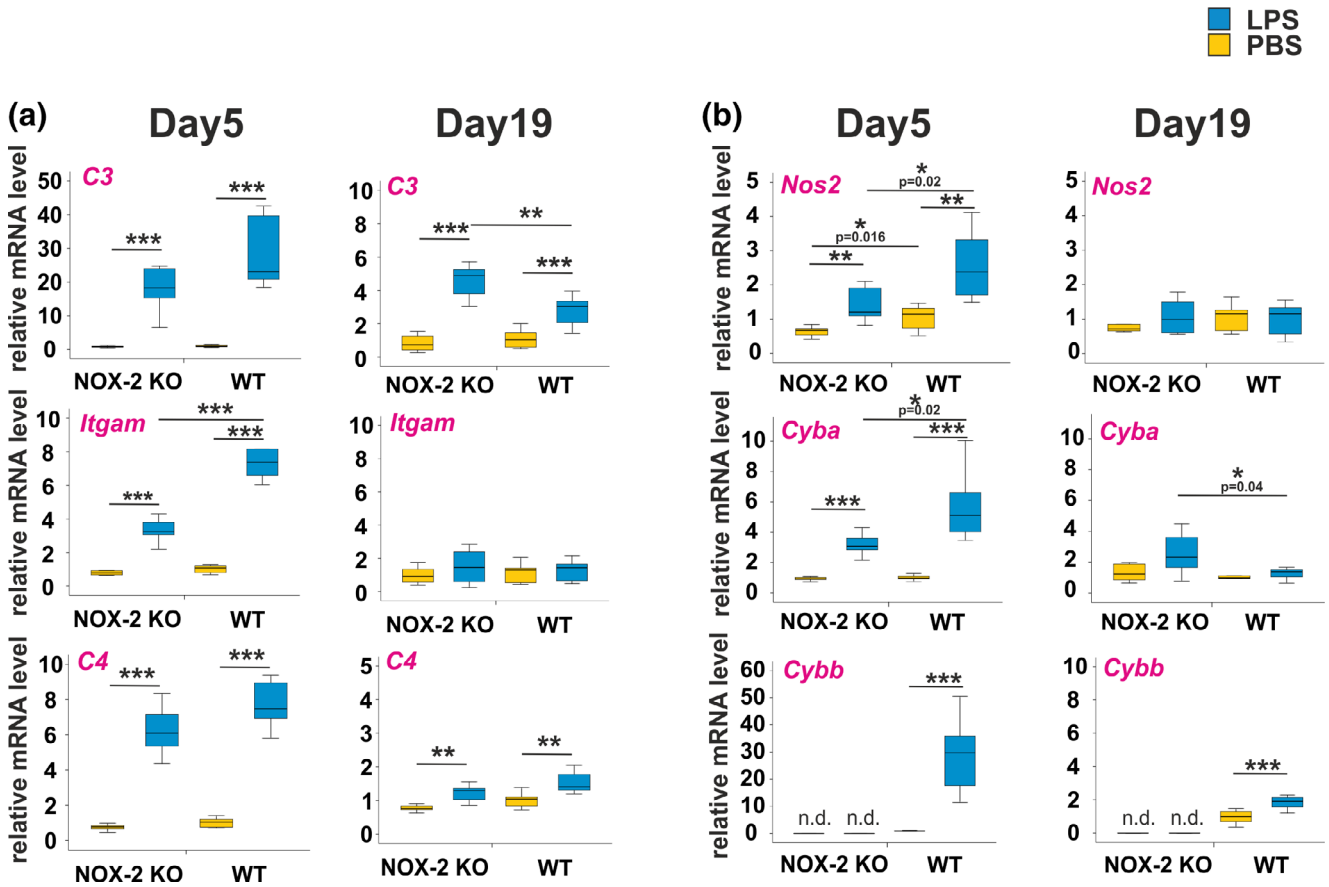

FIGURE 2 Gene transcription levels of complement and radical production pathway molecules after LPS challenge. (a). *C3*, *Itgam*, and *C4* were selected to study the changes in complement pathway molecules expression upon LPS treatment in WT versus NOX-2 KO mice at Day 5 and Day 19. LPS raised their transcript levels in both genotypes. (b). For radical production pathway changes, *Nos2*, *Cyba*, and *Cybb* transcript levels were investigated at Day 5 and 19. LPS raised their transcript levels in both genotypes, but significantly higher in WT compare to NOX-2 KO. Data are shown as boxplot (min./Q1/median/Q3/max.) of $n \geq 9$ mice. One-way ANOVA followed by Dunnett-T3 post hoc test; $^{*}p < .05$. $^{**}p < .01$. $^{***}p < .001$. n.d, not detectable

to 7.9 ± 0.6 (mean ± SEM; $p < .001$; Figure 2a); and in NOX-2 KO genotype this level increased from 0.8 ± 0.05 to 3.42 ± 0.25 (mean ± SEM; $p < .001$; Figure 2a). The increased level of *Itgam* mRNA transcripts upon LPS treatment was higher in WT genotype compare to NOX-2 KO genotype ($p < .001$; Figure 2a). For *C4* in WT genotype, the mRNA transcripts level increased from 1.02 ± 0.08 to 7.8 ± 0.4 (mean ± SEM; $p < .001$; Figure 2a); and in NOX-2 KO genotype this level increased from 0.7 ± 0.06 to 6.3 ± 0.4 (mean ± SEM; $p < .001$; Figure 2a). Interestingly, *C3* and *C4* transcripts level in both genotypes stayed higher in LPS injected mice compare to PBS controls at Day 19 (*C3* transcripts 1.1 ± 0.17 to 2.8 ± 0.3 in WT, and 0.8 ± 0.14 to 4.5 ± 0.3 in NOX-2 KO; *C4* transcripts 1.02 ± 0.07 to 1.52 ± 0.1 in WT, and 0.77 ± 0.02 to 1.2 ± 0.07 in NOX-2 KO).

In addition, nitric oxide 2 (*Nos2*), and the two subunits of NADPH oxidase complex, namely cytochrome b-245 alpha chain (*Cyba*), and cytochrome b-245 heavy chain (*Cybb*), were selected to study alteration in radical production pathway. On Day 5, the mRNA transcripts levels of *Nos2* and *Cyba* increased in LPS challenged mice compared to PBS control in both genotypes. For *Nos2* in WT genotype, transcription levels increased from 1.05 ± 0.1 to 2.57 ± 0.3 (mean ± SEM; $p = .004$; Figure 2b); and in NOX-2 KO genotype this level increased from 0.64 ± 0.05 to 1.4 ± 0.1 (mean ± SEM; $p = .005$; Figure 2b). The increased level of *Nos2* mRNA transcripts upon LPS treatment was higher in WT genotype compared to NOX-2 KO genotype (mean ± SEM; $p = .025$; Figure 2b). For *Cyba* in WT genotype, transcription levels increased from 1.02 ± 0.06 to 5.6 ± 0.6 (mean ± SEM; $p < .001$; Figure 2b); and in NOX-2 KO genotype this level increased from 0.9 ± 0.04 to 3.14 ± 0.21 (mean ± SEM; $p < .001$; Figure 2b). The increased level of *Cyba* mRNA transcripts upon LPS treatment was higher in WT genotype compared to NOX-2 KO genotype ($p = .021$; Figure 2b). For *Cybb* in WT genotype, the mRNA transcripts level increased from 0.91 ± 0.05 to 28.5 ± 4.2 (mean ± SEM; $p < .001$; Figure 2b); and in NOX-2 KO genotype the mRNA was not detectable. This increased level of *Cybb* in WT remained higher even at Day 19 in LPS-treated versus PBS controls (0.9 ± 0.1 to 1.8 ± 0.1; mean ± SEM).

Furthermore, analysis of mRNA transcript levels of selected genes, related to the apoptosis and necroptosis pathways, showed that the Fas-associated protein with death domain (*Fadd*) gene, which is an adaptor protein in apoptosis signaling, was higher expressed at

Day 19 after LPS stimulation in WT mice ($p < .001$) compared to NOX-2 KO mice (Figure S4). Furthermore, *Erk1* (*Mapk3*), another apoptosis signaling related gene and Receptor-interacting serine/threonine-protein kinase (*Ripk3*), one relevant factor of necroptosis induction, were higher expressed in WT compared to NOX-2 KO mice upon LPS stimulation (Figure S4), supporting an increase in apoptosis and necroptosis in WT mice.

In summary, LPS-treatment elevated gene transcript levels of molecules involved in complement (*C3*, *C4*), phagocytic receptor (*Itgam*) and phagocytosis-associated oxidative burst pathways (*Nos2*, *Cyba*, *Cybb*), in both WT and NOX-2 KO genotypes. However, in most cases, this increase was significantly higher in WT compared to NOX-2 KO mice.

3.3 | Inflammation and phagocytosis-related pathways increased upon LPS application

To study changes in inflammatory cytokines, on Day 5, the mRNA transcript levels of tumor necrosis factor-α (*Tnfα*) and Interleukin 1β (*Il1β*) were monitored. Transcripts of *Tnfα* and *Il1β* increased in LPS challenged mice compare to PBS control in both genotypes. For *Tnfα* in WT genotype, transcription levels increased from 1.03 ± 0.09 to 15.2 ± 2.5 (mean ± SEM; $p = .002$; Figure 3a); and in NOX-2 KO genotype this level increased from 1.02 ± 0.1 to 8.34 ± 0.7 (mean ± SEM; $p < .001$; Figure 3a). Similarly, *Il1β* expression in WT genotype increased from 1.08 ± 0.07 to 109.2 ± 23.9 (mean ± SEM; $p = .008$; Figure 3a); and in NOX-2 KO genotype increased from 1.25 ± 0.16 to 62.8 ± 7.8 (mean ± SEM; $p < .001$; Figure 3a). Additional analyses of TLR4 signaling selected genes (*Tlr4*, *Cd14*, and *Myd88*) showed that the *Cd14* gene transcripts (the co-receptor of TLR4 receptor) was transiently increased in response to LPS challenge in WT vs. NOX-2 KO mice (Figure S5).

To study changes in the phagocytosis-related pathway, two molecules TYRO protein tyrosine kinase-binding protein *(Tyrobp/Dap12)* and Fc fragment of IgE, high affinity I, receptor for gamma polypeptide *(Fcer1g)* were selected. For *Dap12* in WT genotype, mRNA levels were elevated from 1.1 ± 0.13 to 5.15 ± 0.6 (mean ± SEM; $p < .001$; Figure 3b); and in NOX-2 KO genotype they were increased from 1.07 ± 0.1 to 3.43 ± 0.3 (mean ± SEM; $p < .001$; Figure 3b). For *Fcer1g* in WT genotype, this level increased from 1.08 ± 0.1 to 6.5 ± 0.6 (mean ± SEM; $p < .001$; Figure 3b); and in NOX-2 KO genotype this level increased from 1 ± 0.06 to 4.3 ± 0.3 (mean ± SEM; $p < .001$; Figure 3b). Interestingly, this increase was significantly higher in WT genotype compared to NOX-2 KO genotype (6.5 ± 0.6 vs 4.33 ± 0.3; $p = .026$; Figure 3b). At Day 19, most of the transcript expression levels returned to amounts comparable to control littermates except for *Il1β*, whose mRNA quantity was higher in both LPS-treated genotypes NOX-2 KO (1.1 ± 0.1 vs 3.3 ± 0.18; mean ± SEM; $p < .001$) and WT (1 ± 0.1 vs 2.7 ± 0.3; mean ± SEM; $p = .004$).

In summary, LPS-treatment raised inflammatory cytokines (*Tnfα* and *Il1β*) and phagocytosis signaling pathway related molecules (*Dap12* and *Fcer1g*) in both WT and NOX-2 KO genotypes, whereas only *Fcer1g* showed a higher increase in WT compared to NOX-2 KO mice.

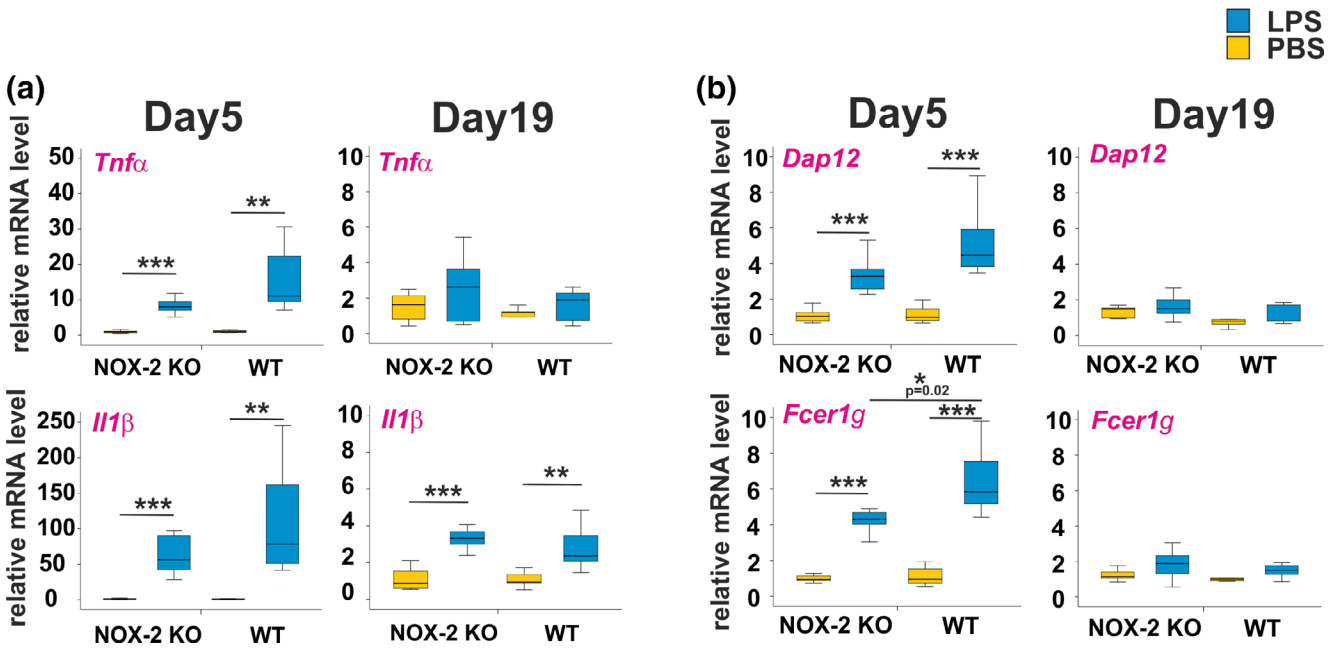

FIGURE 3 Gene transcription levels of inflammatory cytokines and phagocytosis pathway molecules after LPS challenge. (a). For inflammatory pathway *Tnfα* and *Il1β* transcription was investigated upon LPS-treatment in WT versus NOX-2 KO mice at Day 5 and Day 19. LPS raised their transcript levels in both genotypes. (b). For phagocytosis pathway *Dap12* and *Fcer1g* transcript levels were investigated at Day 5 and 19. LPS raised their transcript levels in both genotypes. Data are shown as boxplot (min./Q1/median/Q3/max.) of $n \geq 9$ mice. One-way ANOVA followed by Dunnett-T3 post hoc test; $^{*}p < .05$. $^{**}p < .01$. $^{***}p < .001$

3.4 | Transcription of microglial genes *Cd68* and *Iba1* after repeated, systemic LPS challenge was reduced in NOX-2 KO mice compared to WT mice

Ionized calcium binding adaptor molecule 1 (IBA1), a cytoplasmic protein found only in myeloid phagocytes such as microglia, is known to be evenly distributed in the cellular cytoplasm and thus serves as a good marker of microglial cells. Cluster of Differentiation 68 (CD68), a scavenger receptor, is mainly expressed on lysosomal membranes and presents as a dotted distribution in microglial cells (Hendrickxa, van Edena, Schuurmana, Jörg Hamanna, & Huitinga, 2017; Korzhevskii & Kirik, 2016). Both, IBA1 and CD68 were reported to be upregulated upon LPS activation in mice. TMEM119 was recently described to be exclusively expressed on microglia, with no or low expression found in infiltrating blood-derived macrophages (Bennett et al., 2016). Therefore, to study the microglial response upon LPS challenge, a semi-quantitative real-time PCR analysis for the microglial markers *Cd68*, *Iba1*, and *Tmem119* in whole brain samples was performed.

On Day 5, the mRNA transcripts levels of *Cd68*, *Iba1*, and *Tmem119* were increased in LPS challenged mice compared to PBS control, in both genotypes. For *Cd68* in WT genotype, transcript levels increased from 1.04 ± 0.09 to 6.08 ± 0.43 (mean ± SEM; $p < .001$; Figure 4a); and in NOX-2 KO genotype this level increased from 0.68 ± 0.07 to 2.25 ± 0.2 (mean ± SEM; $p = .002$; Figure 4a). Interestingly, the increased level of Cd*68* mRNA transcripts upon LPS treatment was significantly higher in WT genotype compare to NOX-2 KO genotype ($p < .001$; Figure 4a). For *Iba1* in WT genotype, transcription levels increased from 1.05 ± 0.1 to 4.98 ± 0.5 (mean ± SEM; $p < .001$; Figure 4a); and in NOX-2 KO genotype this level increased from 0.5 ± 0.07 to 2.76 ± 0.25 (mean ± SEM; p < .001; Figure 4a). Again, the increased level of *Iba1* mRNA transcripts upon LPS treatment was significantly higher in WT genotype compare to NOX-2 KO genotype ($p = .012$; Figure 4a). For *Tmem119* in WT genotype, the mRNA transcripts level elevated from 0.94 ± 0.08 to 2.62 ± 0.1 (mean ± SEM; $p < .001$; Figure 4a); and in NOX-2 KO genotype this level raised from 0.8 ± 0.05 to 2.09 ± 0.13 (mean ± SEM; $p < .001$; Figure 4A). However, on Day 19, mRNA transcript levels in LPS treated groups returned to levels comparable with PBS injected controls. The only exception was *Cd68* mRNA levels, which was higher in LPS treated group compared to PBS control in NOX-2 KO genotype (0.9 ± 0.03 vs. 1.2 ± 0.07; mean ± SEM; $p = .03$).

Furthermore, the protein expression of the microglial activation marker CD68 and IBA1 in the substantia nigra pars reticulata (SNpr) was measured via immunohistochemistry that were matched to the bregma levels of the TH and NeuN analyses (Figure 4b). On Day 5, the CD68 and IBA1 immunohistochemistry staining was elevated in LPS treated mice compared to PBS control in both genotypes (Figure 4b). Quantification of the CD68 immunohistochemistry data showed that PBS application in NOX-2 KO (1.1 ± 0.1; mean ± SEM) and WT (1 ± 0.1; mean ± SEM) genotypes showed similar relative intensity staining (Figure 4c), indicating that the loss of NOX-2 had no effect on CD68 expression. However, repeated LPS challenge elevated relative CD68 intensity in NOX-2 KO genotype from 1.1 ± 0.1 to 2.9 ± 0.2 (mean ± SEM; $p < .001$; Figure 4c), and in WT genotype from 1 ± 0.1 to 3.1 ± 0.2 (mean ± SEM; $p < .001$; Figure 4c). On Day 19, there was no difference in CD68 intensity in LPS challenge group compared to PBS control in NOX-2 KO genotype; however, in WT genotype the relative CD68 intensity was still higher in LPS group (1.7 ± 0.1; mean ± SEM) compare to PBS control (1 ± 0.13; $p = .006$; Figure 4c). Likewise, quantification of the IBA1 intensity of the immunohistochemistry showed that PBS application in NOX-2 KO (0.9 ± 0.06; mean ± SEM) and WT (1 ± 0.07; mean ± SEM) genotypes showed similar relative intensity staining (Figure 4c), indicating that the loss of NOX-2 had no effect on IBA1 expression. However, repeated LPS challenge elevated relative IBA1 intensity in NOX-2 KO genotype from 0.9 ± 0.06 to 1.72 ± 0.06 (mean ± SEM; $p < .001$; Figure 4c), and in WT genotype from 1 ± 0.07 to 1.69 ± 0.04 (mean ± SEM; $p < .001$; Figure 4c). Interestingly, the NOX-2 KO mice showed a similar increase of the IBA1 intensity compared to the WT control mice after repeated LPS challenge, indicating that the loss of NOX-2 had no effect on the LPS-induced IBA1 intensity. On Day 19, there was no difference in IBA1 intensity in the LPS challenged groups compared to PBS controls in both genotypes.

Overall, Cd68 (gene transcription and protein expression), Iba1 (gene transcription and protein expression), and *Tmem119* (gene transcription) were increased in both genotypes upon LPS application at Day 5. At Day 19 protein expression of CD68 remained higher in WT mice upon LPS application. Gene transcript levels of *Cd68* and *Iba1* upon LPS treatment were higher in the WT compared to the NOX-2 KO genotype at Day 5.

3.5 | Loss of dopaminergic neurons in the substantia nigra pars compacta induced by repeated systemic LPS application was attenuated in NOX-2 KO mice

To study the involvement of the NADPH oxidase in LPS-triggered loss of dopaminergic neurons, NOX-2 KO mice and WT mice were challenged repeatedly with LPS and analyzed at Day 19 for signs of neurodegeneration. Immunohistochemical stainings of the SN*pc* area were carried out with antibodies against dopaminergic marker tyrosine hydroxylase (TH) and neural nuclei marker NeuN (Figure 5a). Quantification of the immunohistochemistry data was performed at three bregma levels (Figure S6). The average of the relative cell numbers obtained from the three bregma levels showed that the vehicle control PBS applied in mice of both NOX-2 KO (97% ± 4.8%; mean ± SEM) and WT (100% ± 3.6%; mean ± SEM) genotypes showed no significant difference in the relative numbers of TH positive neurons in the SN*pc* area (Figure 5b). In addition, quantification of the relative number of NeuN positive neurons in SN*pc* area confirmed that after PBS application, NOX-2 KO (96.2% ± 5.7%; mean ± SEM) and WT (100% ± 2.4%; mean ± SEM) had no significant difference in neuronal density (Figure 5b), although NeuN positive neurons showed a slight tendency without any statistical significance for reduced numbers in NOX-2 KO compared to WT mice.

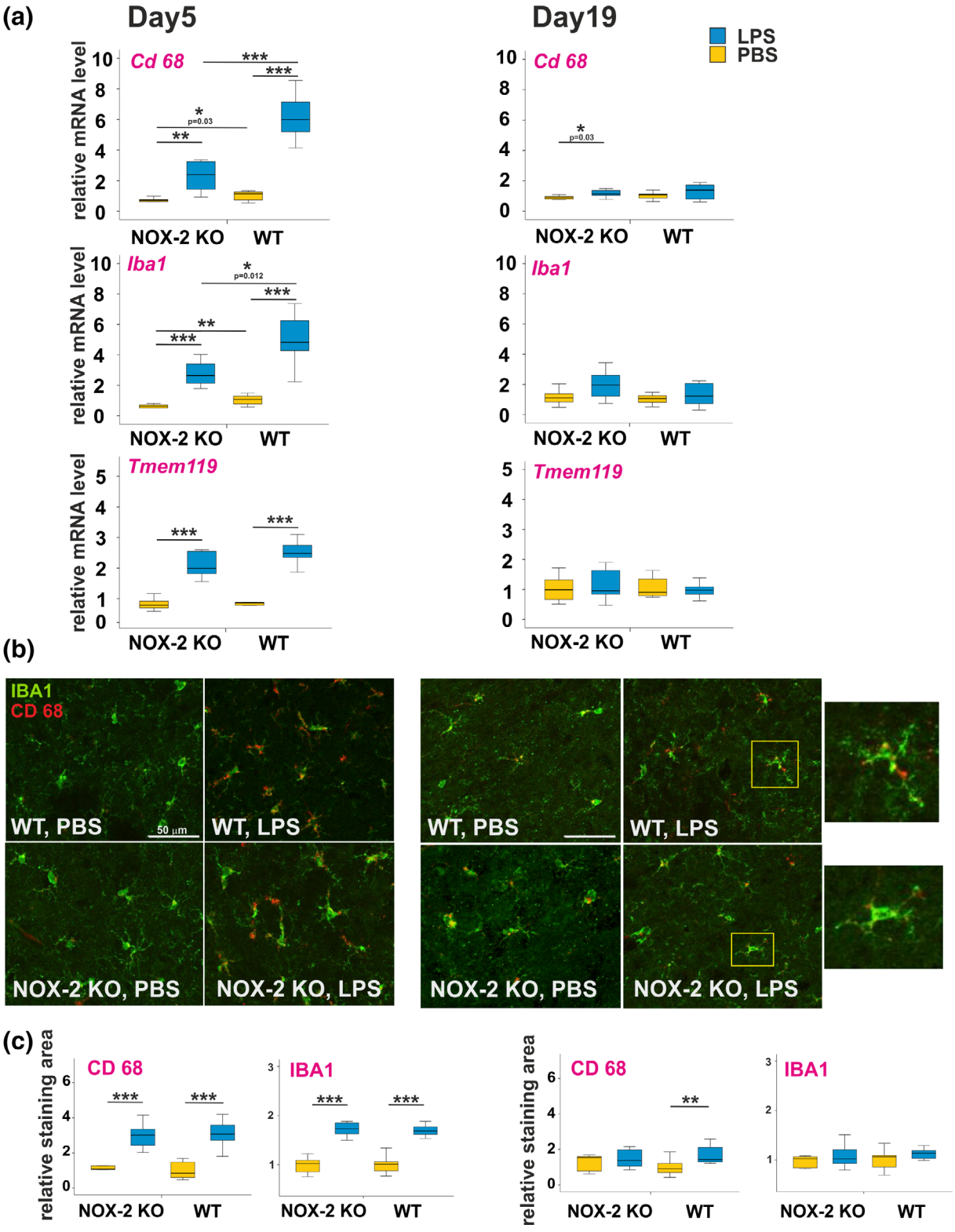

FIGURE 4 Increased microglial activation after LPS treatment. (a). Relative mRNA expression from whole brain sample of mice analyzed on Day 5 (A, left) and on Day 19 (A, right). The mRNA levels of *Cd68*, *Iba1*, and *Tmem119* increased after LPS treatment in both WT and NOX-2 KO genotype and returned to control levels at Day 19. Data are shown as boxplot (min./Q1/median/Q3/max.) $n \geq 9$ mice. One-way ANOVA followed by Dunnett T3 post hoc test for *Cd68* and *Iba1*, Bonferroni post hoc test for *Tmem119*; $^{*}p < .05$. $^{**}p < .01$. $^{***}p < .001$. (b). Representative images of immunohistochemical staining of SN*pr* area stained for microglial marker IBA1 (green) and microglial activation marker CD68 (red) in WT and NOX-2 KO mice injected with LPS or PBS as control for experiments on Day 5 (b, left) and for experiments on Day 19 (b, right). Scale bar: 50 µm. (c). Quantification of CD68 and IBA1 immunostaining in SN*pr* area on Day 5 and on Day 19. In both genotypes, LPS challenge led to increase in CD68 and IBA1 immunoreactivity, and returns to control level on Day 19 (for CD68 only in NOX-2 KO). Data are shown as boxplot (min./Q1/median/Q3/max.) of $n \geq 7$ mice. One-way ANOVA followed by Bonferroni post hoc test; $^{*}p < .05$. $^{**}p < .01$. $^{***}p < .001$

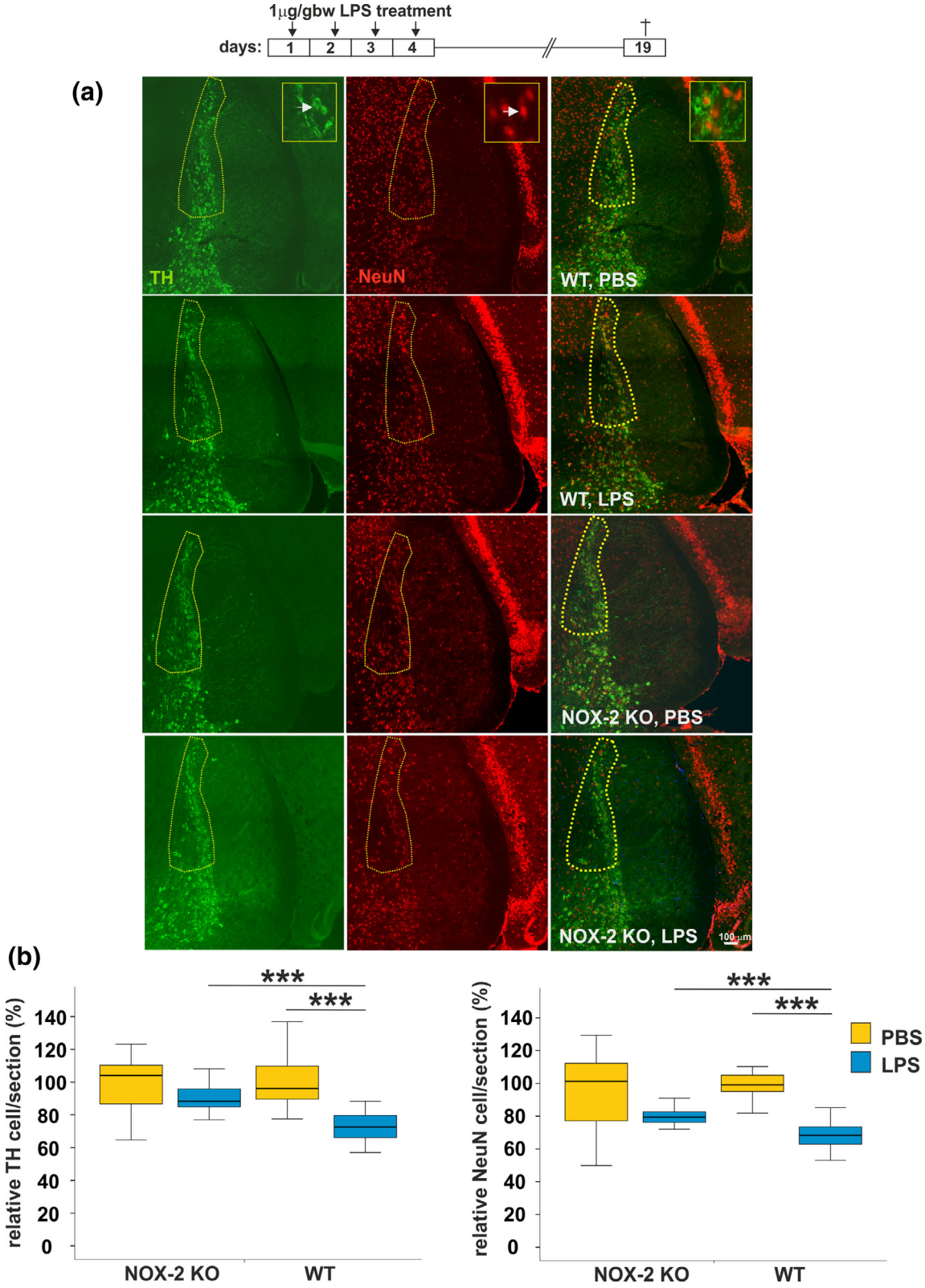

FIGURE 5 Loss of dopaminergic neurons in SN area upon repeated LPS injection. Mice were injected on four consecutive days intraperitoneally with LPS (1 μg/gbw/day) or PBS as control, and analyzed on Day 19. (a). Representative images of immunohistochemical staining of SN area stained for dopaminergic marker TH (green) and neural nuclei marker NeuN (red), in WT and NOX-2 KO mice at bregma −2.92 mm. Scale bar: 100 μm. (b). Quantification of TH positive cells (b, left) and NeuN positive cells (b, right) in SN*pc* area on Day 19. Only in WT genotype LPS challenge led to significant reduction in TH and NeuN positive cells. Data are shown as boxplot (min./Q1/median/Q3/max.) of the average of the relative cell number per section from the three analyzed bregma levels of $n = 9$ mice per experimental group. One-way ANOVA followed by Dunnett T3 post hoc test; ***$p < .001$

Repeated systemic challenge with LPS showed a loss of neurons in WT genotype with a reduction of the relative number of TH positive neurons from 100% ± 3.6% to 73% ± 2.1% (mean ± SEM; $p < .001$; Figure 5b), which was also evident for NeuN positive neurons that were reduced from 100% ± 2.4% to 69% ± 1.9% (mean ± SEM; $p < .001$; Figure 5b). In NOX-2 KO genotype, the reduction of TH positive neurons after LPS treatment (91.2% ± 2.5%; mean ± SEM) was not as prominent as in the WT genotype (73% ± 2.1%; mean ± SEM; $p < .001$). Again, the reduction of NeuN positive neurons in mice challenged with LPS with a NOX-2 KO genotype (81.5% ± 2.2%; mean ± SEM) was much less pronounced when compared to the mice with a WT genotype (69% ± 1.9%; mean ± SEM; $p = .001$), showing that NOX-2 deficiency reduced the loss of neurons triggered by the LPS application.

In summary, mice with a NOX-2 deficiency showed less reduction in TH and NeuN positive neurons in the SN*pc* area compared to WT mice after repeated, systemic LPS challenge.

4 | DISCUSSION

In this study we analyzed the role of microglial phagocytosis-related NOX-2 using *Cybb*-deficient mice and found less LPS-induced neurodegeneration in the SN*pc* of NOX-2 KO compared to WT control mice. Whole genome transcript analysis by RNA-seq of mouse brains after LPS challenge showed that the main difference in gene transcription was related to the LPS injection (75.7% variance explained by PC1 corresponding to LPS versus PBS treatment), while the influence of genotype only showed a minor contribution to the observed variance (8.2% variance explained by PC2 corresponding to NOX-2 KO versus WT; Figure 1a). Furthermore, under repeated systemic challenge with LPS and presence of activated microglial cells, NOX-2 KO mice showed attenuated neurodegeneration. Reduced loss of neurons in NOX-2 KO mice after repeated LPS challenge was associated with lower gene transcripts of lysosome, phagosome, apoptosis and necroptosis pathways in mouse brains. We did not observe a significant difference in neuronal density in the SN*pc* of WT and NOX-2 KO mice without LPS stimuli, but TH positive and NeuN positive neurons showed a slight tendency for reduced numbers in NOX-2 KO compared to WT mice. This might be explained by NOX2-generated production of ROS possibly playing a role in neural development, as shown previously (Nayernia et al., 2017; Oswald, Garnham, Sweeney, & Landgraf, 2018).

The exact sequence of events leading to neurodegeneration triggered by the LPS stimulus is unclear. Upon LPS challenge, NOX-2 derived ROS might lead to an unbalanced oxidative response and additional inflammatory changes in the brain of LPS-treated mice, but NOX-2 could also only be indirectly involved in the neurodegeneration. Previously, we showed that a complement-related pathway was associated with loss of nigrostriatal neurons in mice after repeated systemic application of LPS, which caused a significant increase in brain *Tnfα* and *Nos2* gene transcripts in comparison to single LPS injection (Bodea et al., 2014). Along with our previous studies, we now confirmed increased brain transcription of *Tnfα*, *Nos2*, and *Cyba* in both, WT and NOX-2 KO mice after LPS challenge. However, upregulation of *Nos2* and *Cyba*, but not *Tnfα*, was significantly higher in WT than NOX-2 KO mice. Considering that NOX-2 KO mice lack *Cybb*, this indicates an overall unbalanced oxidative response in the brain of LPS-treated mice, which might lead to more damage in WT compared to NOX-2 KO genotype. In response to endotoxins (like LPS), mononuclear phagocytes can be stimulated to release increased levels of *Tnfα* (Parameswaran & Patial, 2010). Particularly, chronic LPS exposure leads to prolonged high levels of *Tnfα* in the microenvironment (Bodea et al., 2014; Vernooy, Dentener, Van Suylen, Buurman, & Wouters, 2002), and phagocytes exposed to such proinflammatory cytokines show NOX-2 complex formation and release of ROS, which can in turn stimulate more cytokine production in a positive feedback loop (Kim, Morgan, Choksi, & Liu, 2007; Tang, Kang, Vanden Berghe, Vandenabeele, & Kroemer, 2019). Dysregulated NO•/ROS/RNS balance aligned with increased levels of *Tnfα* have been shown as sign of persistence inflammation that was followed by apoptosis or necroptosis (Dhuriya & Sharma, 2018). In the present study, the KEGG gene set enrichment analysis also suggested increased activation of necroptosis and apoptosis pathways in WT compared to NOX-2 KO LPS-treated mice. The link between NOX-2 and necroptosis or apoptosis of neurons is unclear, but LPS often induce *Nos2* transcription, which increases NO• release (Arimoto & Bing, 2003; Fonseca et al., 2003; Medeiros et al., 2007). The produced NO• and ROS released from the NOX-2 oxidase can form highly toxic RNS like peroxynitrite, which could directly lead to neurodegeneration (Dias, Junn, & Mouradian, 2013; Dingjan et al., 2016; Schiavone et al., 2019).

Moreover, in our studies we observed higher Ras-related C3 botulinum toxin substrate 1 (*Rac-1*) in WT compare to NOX-2 KO mice upon LPS stimulation (Figure S3). The NOX-2 oxidase consists of membrane bound (CYBB, CYBA) and cytosolic subunits ($p67^{phox}$, $p47^{phox}$, $p40^{phox}$, Rac1/2), and assembly of these units is necessary for function of the NOX-2 oxidase (Akbar et al., 2018). Binding of the GTPase RAC-1 to $p67^{phox}$ has a crucial role in this process (Akbar et al., 2018; Zhou et al., 2012). Elevated RAC-1 activity in microglial cells, can lead to activation of the RAC-1—NOX-2 pathway, release of ROS and subsequent neurodegeneration (Stankiewicz & Linseman, 2014). In addition, macrophages respond to LPS stimulation via RAC-1 activation to induce NFκB-mediated TNFα release (Sanlioglu et al., 2001). Hampering the RAC-1 - NOX-2 pathway via suppressing RAC-1 activation was enough to silence microglial cells and reduce pro-inflammatory cytokine production of TNFα and IL1β (Liu et al., 2019). Therefore, increased RAC-1 transcription, as we observed in WT mice after LPS-challenge, might indirectly support a role of ROS/RNS in neurodegeneration.

Furthermore, KEGG gene set enrichment analysis in this study showed increased activation of the lysosome and phagocytosis pathway in WT but not in NOX-2 KO mice upon LPS challenge. Therefore, we had a closer look at the major lysosomal membrane protein CD68 by RT-PCR and immunostaining analysis. The transcript and the protein levels were increased upon LPS application in both genotypes.

Interestingly, the analysis of CD68 protein expression in IBA1-positive microglial cells revealed persistent high expression of CD68 at Day 19 in WT mice, which indicates prolonged lysosomal activity in WT compared to NOX-2 KO mice. Thus, increased neurodegeneration in WT mice was associated with higher lysosomal activity of microglial cells, indicative of removal of dopaminergic neurons by phagocytosis as described in previous literature (Marinova-Mutafchieva et al., 2009). In addition to higher *Cd68* transcripts, we observed higher *Iba1* transcripts in WT compared to NOX-2 KO mice, and immunostainings confirmed that protein expression levels followed the changes in gene transcriptions. Interestingly, IBA1 through its actin binding function might be involved in phagocytosis function of microglia (Ohsawa, Imai, Sasaki, & Kohsaka, 2004). These results also suggest that the activated microglia may remove apoptotic or necroptotic neurons from SN*pc* area via phagocytosis. But, we cannot exclude that a slightly increased microglial proliferation upon LPS challenge was responsible for the elevated *Iba1* transcripts levels in WT mice compared to NOX-2 KO mice, since one study has described changes in microglial proliferation in old NOX-2 KO mice with an age of 20–22 months (Geng, Fan, Liu, Smith, & Li, 2020).

In the current study, top enriched Reactome pathways confirmed the involvement of the complement cascade in LPS challenged mice. This is in alignment with our previous data showing a critical role of C3 in neurodegeneration triggered by repeated systemic LPS application (Bodea et al., 2014). In addition, we confirmed increased transcript levels of *C3*, *C4*, and *Itgam* upon LPS-application at Day 5 in both genotypes by RT-PCR. Moreover, the *Itgam* transcripts were significantly higher in WT compared to NOX-2 KO mice. Recently, it is reported that the metabolite 2,5-hexanedione caused dopaminergic neurodegeneration in rats via integrin $\alpha_M\beta_2$ (CR3) involvement, Src-ERK pathway, and NOX-2 activation (C. Zhang et al., 2018). Interestingly, ITGAM (CR3A) inhibition as a regulator of NOX2 activation via Src-ERK pathway in microglial cells could protect dopaminergic neurons from inflammatory damage (Hou et al., 2018). Accordingly, complement components, especially C3, and the complement / phagocytosis receptor Itgam/CR3 together with high Cyba and Cybb expression involved in the oxidative burst are primary suspects for triggering neurodegeneration.

In this study, the immunoreceptor tyrosine-based activation motif (ITAM)-bearing proteins (*Dap12*, *Fcer1g*) gene transcripts were increased upon LPS-application in both genotypes, but with higher magnitude in WT mice. The ITAM has a key regulatory role in microglia and its increased expression upon LPS injection most likely indicates priming of microglia toward an activatory phenotype. TREM2 signaling via ITAMs of TYROBP/DAP12 has a critical role in switching microglial phenotype from a homeostatic state into a disease-associated state (Konishi & Kiyama, 2018). This crucial role of the ITAM signaling pathway has been also elucidated for late onset Alzheimer's disease (Zhang et al., 2013). Recently, a WGCNA-based study confirmed that ITAM-associated microglial genes like TYROBP/DAP12 and FCER1G are major players in neurodegenerative diseases (Mukherjee, Klaus, Pricop-Jeckstadt, Miller, & Struebing, 2019). Furthermore, activation of ITAM-bearing molecules can cause phagocytic signaling with high NADPH oxidase activation and neurodegeneration (Arthur et al., 2012; Konishi & Kiyama, 2018; Nguyen, Green, & Mecsas, 2017).

Based on the microenvironment and context, presence of ROS can lead to either survival or death (Blaser, Dostert, Mak, & Brenner, 2016; Han, Ybanez, Ahmadi, Yeh, & Kaplowitz, 2009). While oxidative burst by phagocytes might be detrimental to postmitotic neurons as observed in our study, lack of the same pathway was related to spontaneous autoimmunity and type I IFN signature in proliferative immune cells (Belarbi, Cuvelier, Destée, Gressier, & Chartier-Harlin, 2017; Kelkka et al., 2014). Thus, the pro-oxidative effects of phagocyte NOX-2 can restrict highly proliferative and renewing immune cell types in immune organs, while triggering neurodegeneration in the brain.

In summary, data show that three major microglial phagocytosis-related components are suspected to be involved in neurodegeneration triggered by systemic LPS application: (a) complement, (b) phagocytosis/lysosomes, and (c) necroptosis/apoptosis. It is likely that a combination of all three microglial phagocytosis-related pathways are involved in the loss of neurons. However, based on this study the NOX-2 complex is one of the major players in this process since NOX-2 KO mice showed less neurodegeneration compared to WT mice.

ACKNOWLEDGMENT

This project was supported by the DFG-funded excellence cluster "ImmunoSensation" (EXC 1023). We thank the Next Generation Sequencing (NGS) Core Facility of the Medical Faculty of the University of Bonn for the generation of the sequencing data. We thank Vibha Anantha Simha, Rita Jietou, and Annemarie Bungartz for excellent technical support. Open access funding enabled and organized by Projekt DEAL.

DATA AVAILABILITY STATEMENT

The data that support the findings of this study are available from the corresponding author upon reasonable request.

ORCID

Harald Neumann https://orcid.org/0000-0002-5071-5202

REFERENCES

Akbar, H., Duan, X., Piatt, R., Saleem, S., Davis, A. K., Tandon, N. N., … Zheng, Y. (2018). Small molecule targeting the Rac1-NOX2 interaction prevents collagen-related peptide and thrombin-induced reactive oxygen species generation and platelet activation. *Journal of Thrombosis and Haemostasis*, *16*(10), 2083–2096. https://doi.org/10.1111/jth.14240

Arimoto, T., & Bing, G. (2003). Up-regulation of inducible nitric oxide synthase in the substantia nigra by lipopolysaccharide causes microglial activation and neurodegeneration. *Neurobiology of Disease*, *12*, 35–45. https://doi.org/10.1016/S0969-9961(02)00017-7

Arthur, J. F., Qiao, J., Shen, Y., Davis, A. K., Dunne, E., Berndt, M. C., … Andrews, R. K. (2012). ITAM receptor-mediated generation of reactive oxygen species in human platelets occurs via Syk-dependent and Syk-independent pathways. *Journal of Thrombosis and Haemostasis*, *10*(6), 1133–1141. https://doi.org/10.1111/j.1538-7836.2012.04734.x

Belarbi, K., Cuvelier, E., Destée, A., Gressier, B., & Chartier-Harlin, M. C. (2017). NADPH oxidases in Parkinson's disease: A systematic review.

Molecular Neurodegeneration, *12*, 84. https://doi.org/10.1186/s13024-017-0225-5

Bennett, M. L., Bennett, F. C., Liddelow, S. A., Ajami, B., Zamanian, J. L., Fernhoff, N. B., … Barres, B. A. (2016). New tools for studying microglia in the mouse and human CNS. *Proceedings of the National Academy of Sciences*, *113*(12), E1738–E1746. https://doi.org/10.1073/PNAS.1525528113

Blaser, H., Dostert, C., Mak, T. W., & Brenner, D. (2016). TNF and ROS crosstalk in inflammation. *Trends in Cell Biology*, *26*(4), 249–261. https://doi.org/10.1016/j.tcb.2015.12.002

Bodea, L. G., Wang, Y., Linnartz-Gerlach, B., Kopatz, J., Sinkkonen, L., Musgrove, R., … Neumann, H. (2014). Neurodegeneration by activation of the microglial complement-phagosome pathway. *Journal of Neuroscience*, *34*(25), 8546–8556. https://doi.org/10.1523/JNEUROSCI.5002-13.2014

Carlson, M. (2019). org.Mm.eg.Db: Genome wide annotation for mouse. R package version 3.8.2. Available at https://doi.org/10.18129/B9.bioc.org.Mm.eg.db

Czapski, G. A., Cakala, M., Chalimoniuk, M., Gajkowska, B., & Strosznajder, J. B. (2007). Role of nitric oxide in the brain during lipopolysaccharide-evoked systemic inflammation. *Journal of Neuroscience Research*, *85*(8), 1694–1703. https://doi.org/10.1002/jnr.21294

Dhuriya, Y. K., & Sharma, D. (2018, July 6). Necroptosis: A regulated inflammatory mode of cell death. *Journal of Neuroinflammation*, *15*, 199. https://doi.org/10.1186/s12974-018-1235-0

Dias, V., Junn, E., & Mouradian, M. M. (2013). The role of oxidative stress in parkinson's disease. *Journal of Parkinson's Disease*. I O S Press, *3*, 461–491. https://doi.org/10.3233/JPD-130230

Dingjan, I., Verboogen, D. R. J., Paardekooper, L. M., Revelo, N. H., Sittig, S. P., Visser, L. J., … Van Den Bogaart, G. (2016). Lipid peroxidation causes endosomal antigen release for cross-presentation. *Scientific Reports*, *6*, 22064. https://doi.org/10.1038/srep22064

Dobin, A., Davis, C. A., Schlesinger, F., Drenkow, J., Zaleski, C., Jha, S., … Gingeras, T. R. (2013). STAR: Ultrafast universal RNA-seq aligner. *Bioinformatics*, *29*(1), 15–21. https://doi.org/10.1093/bioinformatics/bts635

Fonseca, S. G., Romão, P. R. T., Figueiredo, F., Morais, R. H., Lima, H. C., Ferreira, S. H., & Cunha, F. Q. (2003). TNF-α mediates the induction of nitric oxide synthase in macrophages but not in neutrophils in experimental cutaneous leishmaniasis. *European Journal of Immunology*, *33*(8), 2297–2306. https://doi.org/10.1002/eji.200320335

Geng, L., Fan, L. M., Liu, F., Smith, C., & Li, J.-M. (2020). Nox2 dependent redox-regulation of microglial response to amyloid-β stimulation and microgliosis in aging. *Scientific Reports*, *10*(1), 1582. https://doi.org/10.1038/s41598-020-58422-8

Han, D., Ybanez, M. D., Ahmadi, S., Yeh, K., & Kaplowitz, N. (2009). Redox regulation of tumor necrosis factor signaling. *Antioxidants & Redox Signaling*, *11*(9), 2245–2263. https://doi.org/10.1089/ars.2009.2611

Hendrickxa, D. A. E., van Edena, C. G., Schuurmana, K. G., Jörg Hamanna, B., & Huitinga, I. (2017). Staining of HLA-DR, Iba1 and CD68 in human microglia reveals partially overlapping expression depending on cellular morphology and pathology. *Journal of Neuroimmunology*, *309*, 12–22.

Hou, L., Wang, K., Zhang, C., Sun, F., Che, Y., Zhao, X., … Wang, Q. (2018). Complement receptor 3 mediates NADPH oxidase activation and dopaminergic neurodegeneration through a Src-Erk-dependent pathway. *Redox Biology*, *14*, 250–260. https://doi.org/10.1016/j.redox.2017.09.017

Kelkka, T., Kienhöfer, D., Hoffmann, M., Linja, M., Wing, K., Sareila, O., … Holmdahl, R. (2014). Reactive oxygen species deficiency induces autoimmunity with type 1 interferon signature. *Antioxidants and Redox Signaling*, *21*(16), 2231–2245. https://doi.org/10.1089/ars.2013.5828

Kim, Y.-S., Morgan, M. J., Choksi, S., & Liu, Z.-G. (2007). TNF-induced activation of the Nox1 NADPH oxidase and its role in the induction of necrotic cell death. *Molecular Cell*, *26*(5), 675–687. https://doi.org/10.1016/j.molcel.2007.04.021

Konishi, H., & Kiyama, H. (2018). Microglial TREM2/DAP12 signaling: A double-edged sword in neural diseases. *Frontiers in Cellular Neuroscience*, *12*, 206. https://doi.org/10.3389/fncel.2018.00206

Korotkevich, G., Sukhov, V., & Sergushichev, A. (2019). Fast gene set enrichment analysis. *bioRxiv 060012*. https://doi.org/10.1101/060012.

Korzhevskii, D. E., & Kirik, O. V. (2016). Brain microglia and microglial markers. *Neuroscience and Behavioral Physiology*, *46*(3), 284–290. https://doi.org/10.1007/s11055-016-0231-z

Liao, Y., Smyth, G. K., & Shi, W. (2014). FeatureCounts: An efficient general purpose program for assigning sequence reads to genomic features. *Bioinformatics*, *30*(7), 923–930. https://doi.org/10.1093/bioinformatics/btt656

Liu, W., Huang, J., Doycheva, D., Gamdzyk, M., Tang, J., & Zhang, J. H. (2019). RvD1binding with FPR2 attenuates inflammation via Rac1/NOX2 pathway after neonatal hypoxic-ischemic injury in rats. *Experimental Neurology*, *320*, 112982. https://doi.org/10.1016/j.expneurol.2019.112982

Love, M. I., Huber, W., & Anders, S. (2014). Moderated estimation of fold change and dispersion for RNA-seq data with DESeq2. *Genome Biology*, *15*(12), 550. https://doi.org/10.1186/s13059-014-0550-8

Marinova-Mutafchieva, L., Sadeghian, M., Broom, L., Davis, J. B., Medhurst, A. D., & Dexter, D. T. (2009). Relationship between microglial activation and dopaminergic neuronal loss in the substantia nigra: A time course study in a 6-hydroxydopamine model of Parkinson's disease. *Journal of Neurochemistry*, *110*(3), 966–975. https://doi.org/10.1111/j.1471-4159.2009.06189.x

Medeiros, R., Prediger, R. D. S., Passos, G. F., Pandolfo, P., Duarte, F. S., Franco, J. L., … Calixto, J. B. (2007). Connecting TNF-α signaling pathways to iNOS expression in a mouse model of Alzheimer's disease: Relevance for the behavioral and synaptic deficits induced by amyloid β protein. *Journal of Neuroscience*, *27*(20), 5394–5404. https://doi.org/10.1523/JNEUROSCI.5047-06.2007

Mukherjee, S., Klaus, C., Pricop-Jeckstadt, M., Miller, J. A., & Struebing, F. L. (2019). A microglial signature directing human aging and neurodegeneration-related gene networks. *Frontiers in Neuroscience*, *13*(JAN), 1–12. https://doi.org/10.3389/fnins.2019.00002

Nayernia, Z., Colaianna, M., Robledinos-Antón, N., Gutzwiller, E., Sloan-Béna, F., Stathaki, E., … Krause, K. H. (2017). Decreased neural precursor cell pool in NADPH oxidase 2-deficiency: From mouse brain to neural differentiation of patient derived iPSC. *Redox Biology*, *13*, 82–93. https://doi.org/10.1016/j.redox.2017.04.026

Nguyen, G. T., Green, E. R., & Mecsas, J. (2017). Neutrophils to the ROScue: Mechanisms of NADPH oxidase activation and bacterial resistance. *Frontiers in Cellular and Infection Microbiology*, *7*, 373. https://doi.org/10.3389/fcimb.2017.00373

Ohsawa, K., Imai, Y., Sasaki, Y., & Kohsaka, S. (2004). Microglia/macrophage-specific protein Iba1 binds to fimbrin and enhances its Actin-bundling activity. *Journal of Neurochemistry*, *88*(4), 844–856. https://doi.org/10.1046/j.1471-4159.2003.02213.x

Oswald, M. C. W., Garnham, N., Sweeney, S. T., & Landgraf, M. (2018, March 1). Regulation of neuronal development and function by ROS. *FEBS Letters*, *592*, 679–691. https://doi.org/10.1002/1873-3468.12972

Parameswaran, N., & Patial, S. (2010). Tumor necrosis factor-α signaling in macrophages.

Perry, V. H., Cunningham, C., & Holmes, C. (2007). Systemic infections and inflammation affect chronic neurodegeneration. *Nature Immunology*, *7*, 161–167.

Qin, L., Liu, Y., Hong, J. S., & Crews, F. T. (2013). NADPH oxidase and aging drive microglial activation, oxidative stress, and dopaminergic neurodegeneration following systemic LPS administration. *Glia*, *61*(6), 855–868. https://doi.org/10.1002/glia.22479

Qin, L., Wu, X., Block, M. L., Liu, Y., Breese, G. R., Hong, J. S., … Crews, F. T. (2007). Systemic LPS causes chronic neuroinflammation and progressive neurodegeneration. *Glia*, *55*(5), 453–462. https://doi.org/10.1002/glia.20467

Sanlioglu, S., Williams, C. M., Samavati, L., Butler, N. S., Wang, G., McCray, P. B., … Engelhardt, J. F. (2001). Lipopolysaccharide induces Rac1-dependent reactive oxygen species formation and coordinates tumor necrosis factor-α secretion through IKK regulation of NF-κB. *Journal of Biological Chemistry*, *276*(32), 30188–30198. https://doi.org/10.1074/jbc.M102061200

Schiavone, S., Neri, M., Maffione, A. B., Frisoni, P., Morgese, M. G., Trabace, L., & Turillazzi, E. (2019). Increased iNOS and nitrosative stress in dopaminergic neurons of MDMA-exposed rats. *International Journal of Molecular Sciences*, *20*(5), 1242. https://doi.org/10.3390/ijms20051242

Stankiewicz, T. R., & Linseman, D. A. (2014). Rho family GTPases: Key players in neuronal development, neuronal survival, and neurodegeneration. *Frontiers in Cellular Neuroscience*, *8*, 314. https://doi.org/10.3389/fncel.2014.00314

Tang, D., Kang, R., Vanden Berghe, T., Vandenabeele, P., & Kroemer, G. (2019). The molecular machinery of regulated cell death. *Cell Research*, *29*, 347–364. https://doi.org/10.1038/s41422-019-0164-5

Vernooy, J. H. J., Dentener, M. A., Van Suylen, R. J., Buurman, W. A., & Wouters, E. F. M. (2002). Long-term Intratracheal lipopolysaccharide exposure in mice results in chronic lung inflammation and persistent pathology. *American Journal of Respiratory Cell and Molecular Biology*, *26*. Retrieved from www.atsjournals.org, 152–159.

Wickham, H. (2016). *ggplot2: Elegant graphics for data analysis*. New York: Springer-Verlag.

Wyss-Coray, T., & Rogers, J. (2012). Inflammation in Alzheimer disease-a brief review of the basic science and clinical literature. *Cold Spring Harbor Perspectives in Medicine*, *2*(1), a006346. https://doi.org/10.1101/cshperspect.a006346

Yu, G., & He, Q. Y. (2016). ReactomePA: An R/bioconductor package for reactome pathway analysis and visualization. *Molecular BioSystems*, *12*(2), 477–479. https://doi.org/10.1039/c5mb00663e

Yu, G., Wang, L. G., Han, Y., & He, Q. Y. (2012). ClusterProfiler: An R package for comparing biological themes among gene clusters. *OMICS A Journal of Integrative Biology*, *16*(5), 284–287. https://doi.org/10.1089/omi.2011.0118

Zhang, B., Gaiteri, C., Bodea, L.-G., Wang, Z., McElwee, J., Podtelezhnikov, A. A., … Emilsson, V. (2013). Integrated systems approach identifies genetic nodes and networks in late-onset Alzheimer's disease. *Cell*, *153*(3), 707–720. https://doi.org/10.1016/j.cell.2013.03.030

Zhang, C., Hou, L., Yang, J., Che, Y., Sun, F., Li, H., & Wang, Q. (2018). 2,5-Hexanedione induces dopaminergic neurodegeneration through integrin αMβ2/NADPH oxidase axis-mediated microglial activation. *Cell Death and Disease*, *9*(2), 60. https://doi.org/10.1038/s41419-017-0091-7

Zheng, H. F., Yang, Y. P., Hu, L. F., Wang, M. X., Wang, F., Cao, L. D., … Liu, C. F. (2013). Autophagic impairment contributes to systemic inflammation-induced dopaminergic neuron loss in the midbrain. *PLoS One*, *8*(8). https://doi.org/10.1371/journal.pone.0070472

Zhou, H., Zhang, F., Chen, S. H., Zhang, D., Wilson, B., Hong, J. S., & Gao, H. M. (2012). Rotenone activates phagocyte NADPH oxidase by binding to its membrane subunit gp91 phox. *Free Radical Biology and Medicine*, *52*(2), 303–313. https://doi.org/10.1016/j.freeradbiomed.2011.10.488

Zhu, A., Ibrahim, J. G., & Love, M. I. (2019). Heavy-tailed prior distributions for sequence count data: Removing the noise and preserving large differences. *Bioinformatics*, *35*(12), 2084–2092. https://doi.org/10.1093/bioinformatics/bty895

SUPPORTING INFORMATION

Additional supporting information may be found online in the Supporting Information section at the end of this article.

How to cite this article: Shahraz A, Wißfeld J, Ginolhac A, Mathews M, Sinkkonen L, Neumann H. Phagocytosis-related NADPH oxidase 2 subunit gp91phox contributes to neurodegeneration after repeated systemic challenge with lipopolysaccharides. *Glia*. 2020;1–14. https://doi.org/10.1002/glia.23890